



Article

Biopolymer-Based Mixed Matrix Membranes (MMMs) for CO₂/CH₄ Separation: Experimental and Modeling Evaluation

Andrea Torre-Celeizabal, Clara Casado-Coterillo *  and Aurora Garea 

Department of Chemical and Biomolecular Engineering, Universidad de Cantabria, 39005 Santander, Spain; torrea@unican.es (A.T.-C.); gareaa@unican.es (A.G.)

* Correspondence: casadoc@unican.es; Tel.: +34-942-20-6777

Abstract: Alternative materials are needed to tackle the sustainability of membrane fabrication in light of the circular economy, so that membrane technology keeps playing a role as sustainable technology in CO₂ separation processes. In this work, chitosan (CS)-based mixed matrix thin layers have been coated onto commercial polyethersulfone (PES) supports. The CS matrix was loaded by non-toxic 1-Ethyl-3-methylimidazolium acetate ionic liquid (IL) and/or laminar nanoporous AM-4 and UZAR-S3 silicates prepared without costly organic surfactants to improve CO₂ permselectivity and mechanical robustness. The CO₂/CH₄ separation behavior of these membranes was evaluated experimentally at different feed gas composition (CO₂/CH₄ feed mixture from 20:80 to 70:30%), covering different separation applications associated with this separation. A cross-flow membrane cell model built using Aspen Custom Modeler was used to validate the process performance and relate the membrane properties with the target objectives of CO₂ and CH₄ recovery and purity in the permeate and retentate streams, respectively. The purely organic IL-CS and mixed matrix AM-4:IL-CS composite membranes showed the most promising results in terms of CO₂ and CH₄ purity and recovery. This is correlated with their higher hydrophilicity and CO₂ adsorption and lower swelling degree, i.e., mechanical robustness, than UZAR-S3 loaded composite membranes. The purity and recovery of the 10 wt.% AM-4:IL-CS/PES composite membrane were close or even surpassed those of the hydrophobic commercial membrane used as reference. This work provides scope for membranes fabricated from renewable or biodegradable polymers and non-toxic fillers that show at least comparable CO₂/CH₄ separation as existing membranes, as well as the simultaneous feedback on membrane development by the simultaneous correlation of the process requirements with the membrane properties to achieve those process targets.



Citation: Torre-Celeizabal, A.; Casado-Coterillo, C.; Garea, A. Biopolymer-Based Mixed Matrix Membranes (MMMs) for CO₂/CH₄ Separation: Experimental and Modeling Evaluation. *Membranes* **2022**, *12*, 561. <https://doi.org/10.3390/membranes12060561>

Academic Editors: Frank Lipnizki and Morten Lykkegaard Christensen

Received: 29 April 2022

Accepted: 26 May 2022

Published: 28 May 2022

Publisher's Note: MDPI stays neutral with regard to jurisdictional claims in published maps and institutional affiliations.



Copyright: © 2022 by the authors. Licensee MDPI, Basel, Switzerland. This article is an open access article distributed under the terms and conditions of the Creative Commons Attribution (CC BY) license (<https://creativecommons.org/licenses/by/4.0/>).

Keywords: chitosan biopolymer-based membranes; CO₂/CH₄ separation; experimental and process simulation

1. Introduction

The concentration of CO₂ in the atmosphere is in continuous growth, by the last century it has increased from 275 to 418 ppm, which has already produced irreversible increases in global temperatures and the concentration of this component is expected to continue to increase over time [1]. Energy production is necessary to face the demand of the growing world population [2]. To face this problem, one possibility is the recovery of biogas to obtain energy [3]. Methane, upgraded from biogas, can be used for heat and electricity production or as biofuel for vehicles to reduce environmental emissions and the use of fossil fuels [4]. Biogas is produced from the methanation of biomass and organic wastes from sewage sludge anaerobic digestion, commercial composting, landfills, biomass gasification, animal, and food waste [5]. Biogas usually contains from 55% to 65% methane, from 35% to 45% carbon dioxide and less than a 1% nitrogen and other traces of sulfur compounds, siloxanes, and aromatic compounds, which can contribute to stratospheric ozone depletion, greenhouse effect, and reduction of the quality of air, as well as cause

corrosion and maintenance problems in the gas pipelines [6]. Carbon dioxide (CO_2) is the other major component of biogas that decreases the density and calorific value of the biogas, thus the importance of separating CH_4 from CO_2 to increase the value and use of biogas as biomethane [5]. Figure 1 shows the different steps in biogas upgrading, with CO_2 removal being the most important cleaning step. CO_2/CH_4 is still a challenging separation due to the variability of the biogas composition, which mainly depends on the source and seasonal conditions as well as the huge amount of water leaving the fermenter that makes necessary a dehydration step in conventional processes, such as chemical absorption [7].

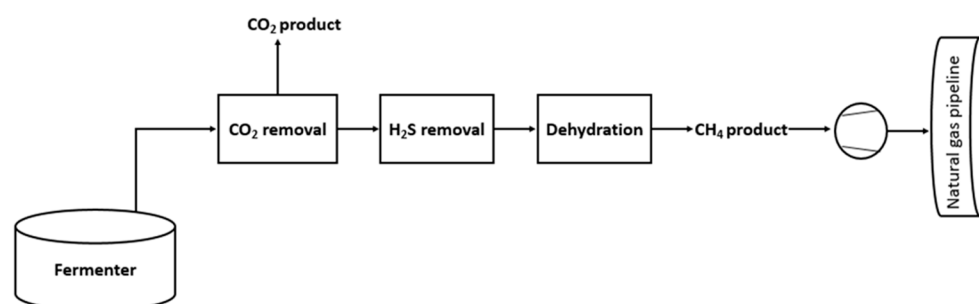


Figure 1. Natural gas upgrading steps adapted from [8].

In this scenario, membrane technology has been selected as one of the efficient technologies to reduce CO_2 emissions in the atmosphere by separation/capture processes from the flue gas, such as natural gas and synthesis gas, achieving sustainable development goals with the creation and utilization of sustainable energy sources [9,10]

The most important properties of membranes to perform this separation are: (1) high CO_2 permeability, (2) high CO_2/CH_4 selectivity, (3) stability of the material, (4) good resistance to aging and plasticization, (5) sustainability and reproducibility of the manufacturing to levelize the fabrication cost upon up-scaling [11]. The most matured membranes for CO_2 separation are based on polymeric materials. Some polymers investigated in literature for CO_2 separation are polysulfone (PSf) [12], polyimide (PI) [13], polyetherimide (PEI) [14,15], polycarbonate (PC) [16,17], polyethersulfone (PES) [18], but the number of CO_2 selective polymer membranes close to commercialization are still limited: Polaris[®], Polyactive[™] and facilitated transport membranes [19]. Even those commercial membranes experience some disadvantages, such as the uncertainty of their performance regarding the presence of impurities, such as water and organic vapors and doubts on the thermal, mechanical, and chemical resistance, as well as the costly fabrication methods [20–22].

Although membrane separation processes are considered eco-friendly technologies, there is still the necessity to improve the sustainability of the membranes themselves using renewable and environmentally friendly materials in their fabrication. Biopolymers can be obtained from various sources and have recently been considered as potential materials for replacing different chemically synthesized polymers used in membrane fabrication due to their properties, such as biocompatibility, biodegradability, compostability and environmental sustainability [11,23,24]. Cellulose acetate (CA) was the first biopolymer to be used for membrane separation because of its properties, such as easy processability, versatility and low environmental footprint. The main disadvantage is that this biopolymer is susceptible to plasticization as a consequence of CO_2 sorption, generally at high pressure [11]. Moghadassi et al. functionalized a CA membrane using multiwalled carbon nanotubes, providing an increase in perm-selectivity compared to pristine CA membranes. Moreover, the addition of organic additives, such as polyethylene glycol (PEG), improved the flexibility of the membrane, implying an increase in permeability and aging resistance [25]. Mubashir et al. incorporated $\text{NH}_2\text{-MIL-53(Al)}$ into a CA matrix, increasing CO_2 permeability from 15.5 Barrer to 52.6 Barrer and CO_2/CH_4 selectivity from 10.7 to 28.7 [26]. Other bio-based polymer materials are becoming more popular in membrane processes (Table A1 in Appendix A). PVA is a synthetic biodegradable, low-cost and

non-toxic polymer with high hydrophilicity and good barrier properties, which is easily blended with other polymers to reduce the crystalline fraction and increase membrane performance [27,28]. Polyvinyl alcohol PVA was blended by polyvinyl amine (PVAm) to provide the selective layer of the membrane with a facilitated transport mechanism and increase the CO₂/CH₄ separation performance regardless of the relative humidity of the fuel gas [29]. PVAm:PVA blend membranes loaded with carbon nanotubes (CNTs) showed improvements on the durability, mechanical resistance, CO₂ permeability and CO₂/CH₄ selectivity compared to the pure polymeric membrane [30]. Jahan et al. coated PVA blended with crystalline nanocellulose (CNC) on a PSf support for biogas upgrading. They observed that the addition of CNC influenced the water swelling degree, crystallinity, and thickness of the resulting membranes, facilitating the transport of CO₂ compared with the pristine PVAm:PVA membrane [31]. Another biopolymer, polyurethane (PU), obtained from polyols in plant oils has been recently reported for gas separation on account of properties of hydrophobicity, low rigidity, stable barrier properties, good mechanical resistance, and water-vapor permeability. Again, the addition of nanoparticles can improve the gas separation performance by increasing free volume as well as thermal and mechanical properties. Molki et al. observed that NiO NPs as filler in PU increased CO₂ permeability while decreasing CH₄ permeability, which is a larger molecule [32]. Ghadimi et al. [33] added PEG to polyurethane and they crosslinked prepared membranes using a methoxysilane-functionalized ionic liquid (Si-IL). The IL used was made from the BF₄⁻ anion with high affinity for CO₂ and the siloxane loading up to 10wt.% increased both the CO₂ permeability and selectivity of the PEG/PU hybrid matrix. The inorganic siloxane domains incorporated into polymeric matrices increases the fractional free volume of the membrane matrix. Pyridinium based ILs have been reported to increase the mechanical stability of CA based membranes in CO₂ separations [34]. Sodeifian et al. [35] used SAPO-34 zeolites as nanoporous fillers in PU MMMs. The differences in kinetic diameter, condensability, and interaction with the polar groups of the polymer and then porosity of the zeolite caused larger increases in the CO₂ permeation rate than that of CH₄. Although these membranes provided a 4.45% and 18.24% reduction of CO₂ and CH₄ permeability, respectively, CO₂/CH₄ selectivity increased about 14.43%. Layered materials have been reviewed to improve gas permeation properties of PES membranes using ionic liquid as a binder between the filler and the continuous matrix [18].

Chitosan (CS) is a non-toxic biopolymer from renewable sources, with low cost, biocompatibility, and high hydrophilicity [36]. CS is a semi-crystalline polymer that contains one hydroxyl group and one amine group in its structure, which are responsible for the facilitated transport of CO₂ across this material [37]. The main properties of biopolymers include high hydrophilicity, low mechanical resistance, variable pore size and membrane morphology [38]. Further, the removal of the impurities in biogas, in particular CO₂, may reduce mass transfer limitations due to the hydrophilic character of the membrane [39]. Fewer studies applied CS-based membranes to CO₂/CH₄ than CO₂/N₂ separation. Jomekian et al. prepared CS modified g-C₃N₄ using PES as porous support and ZIF-8 as filler to increase the performance of the membrane [40]. They observed an increase in selectivity in pure gas experiments when CS-modified was mixed with ZIF-8 compared to ZIF-8 pristine membrane. However, mixed gas experiments showed the same trend, but lower separation factor, due to the competing effects in the penetration of the gases through the membrane [40]. In previous works, 1-ethyl-3-methylimidazolium acetate, [emim][Ac] IL was observed to increase the thermal and mechanical behavior of CS membranes for CO₂/N₂ separation [41]. Mixed-matrix membranes (MMMs) are a well-known route to enhance the properties of polymeric membranes by incorporating an inorganic material in the form of micro- or nanoparticles (filler) into the polymeric matrix (continuous phase) [42]. The addition of ETS.10 titanosilicate [43] and nano-sized ZIF-8 and HKUST-1 particles also improved selectivity and permeability in dense self-standing films on account of the compatibility between the filler and the continuous IL-CS matrix, which we have also studied by Hansen solubility parameters [44]. The successful development of MMMs

depends on the proper selection of the polymer that forms the matrix and the inorganic filler, also on the elimination of interfacial defects between both phases. Another crucial factor is to control filler loading, shape, and size to achieve the best performance [45]. These MMMs can be coated into porous supports that provide mechanical resistance, allowing for the reduction of the thickness of the selective layer and thus increasing membrane productivity without diminishing the selectivity of the self-standing material [46]. The functional groups of the biopolymers and fillers have proven to be useful robust CO₂ carriers in solid facilitated membranes [22]. IL-CS/PES composite membranes using the same IL and HKUST-1 nanoparticles as filler of the CS matrix over a flat polyethersulfone (PES) support [36] or hollow fibers. Furthermore, promising results were obtained for these HKUST-1-CS:IL composite membranes, at a CO₂/CH₄ (50:50v%) feed mixture composition, as selectivity increased from 12 to 30 in wet conditions while CO₂ permeability was maintained at a value of 400 GPU regardless the HKUST-1 loading [47]. Layered AM4-4 and UZAR-S3 silicate materials have proved good interfacial contact with CS-based matrices on account of the compatible ion exchange capacity of both and the high aspect ratio of the 2D nanosheets [48,49] that promotes the CO₂ adsorption capacity of the delaminated AM-4 in comparison with the layered precursor [50] and the thickness of the nanosheet exfoliated layers of UZAR-S3 [51].

This is the reason why these fillers were selected in this study for the preparation of MMM composite membranes based on IL-CS continuous matrix for the selective layer and different fillers ([emim][Ac] IL [41], layered AM-4 titanosilicate [50], layered UZAR-S3 stannosilicate [51] and HKUST-1 metal organic framework (MOF) [44]). The membranes were coated on PES support in order to evaluate the potential to simultaneously increase the permeability, selectivity, and stability of the membranes in a simple way. The performance of the membranes in single gas and CO₂/CH₄ mixture separation was experimentally evaluated at different feed gas mixture compositions and analyzed and compared with other biopolymer-based membranes in the literature using Aspen Custom Modeler. A cross-flow model of membrane cell was validated for the process simulation using a well-known commercial membrane in CO₂ separation applications, by testing different feed gas composition covering different separation scenarios associated with CO₂/CH₄ separation, such as natural gas sweetening, biogas upgrading, and enhanced oil recovery where the gas is richer in CO₂. A sensitivity analysis as a function of the stage-cut as a key process variable was performed and compared with other referenced biopolymer-based membranes.

2. Materials and Methods

2.1. Membrane Preparation

The membranes used for this study are flat-sheet composite membranes synthesized in our laboratory. Commercial PES membranes with a 0.1 μm pore size and a thickness of 132 μm have been used as support for the composite membranes. The top layer coated is made of the chitosan biopolymer (CS) purchased from Sigma Aldrich (Spain) with a few drops (5 wt.% to total solid content) of 1-Ethyl-3-methylimidazolium acetate [emim][Ac] IL (Sigma Aldrich, Spain), after results obtained previously in our research group [41,46]. In brief, prior to the coating of the hydrophilic biopolymer layer, the surface of the PES support was coated by a hydrophobic solution of PDMS/hexane or trimesoyl chloride (TMC)/Hexane 0.1wt.% that prevented cluster or crystallization on the surface pores of the support and allowed a homogeneous coating layer thickness. The IL-CS matrix was loaded by different types of nanometric fillers prepared by a method reported elsewhere (AM-4 [52], UZAR-S3 [53] and HKUST [44]) that have been added to the polymeric membrane in a 10 wt.% of the total mass of the polymer matrix [49]. For the synthesis of the two nanoporous silicates, sodium silicate (Na₂SiO₃), sodium hydroxide (NaOH), Anatase (TiO₂), tin(II) chloride di-hydrated (SnCl₂ 2H₂O) and copper chloride·5 H₂O that were acquired from Aldrich (Spain) were used. Different MMMs were prepared by solution casting at room temperature [44].

The thickness of the prepared membranes was measured by means of a digital Mitutoyo digimatic micrometer (IP 65) with an accuracy of 0.001 mm. The average thickness of the selective layer of the membranes was $43.63 \pm 9.27 \mu\text{m}$ (more details in Table A1, Appendix A). The differences in thickness between the hydrated and dry film allows for monitoring the degree of swelling and the mechanical robustness of the membrane before and after gas separation runs [43]. The experimental density of the membranes (ρ_m) can be measured gravimetrically from the electronically measured weight of the dry film and the volume calculated from the dry thickness at room temperature (20 °C).

The water uptake of the IL-CS based membranes was measured after the activation step in NaOH 1 M and rinsing in DI water. The membranes were immersed in DI water for at least 25 h. The wet weight was obtained by quickly blotting the membrane on tissue paper to remove the excess water. The total water uptake was calculated as:

$$WU(\%) = \frac{W_{wet} - W_{dry}}{W_{dry}} \times 100 \quad (1)$$

where W_{dry} is the dry weight of the membrane, and W_{wet} the weight of the swelling membrane, both in grams. The porosity of the membrane has been calculated as in previous works, from the volume occupied by water and the volume of the membrane, considering the water density at 20 °C (0.998 g/cm³) and the density of the membrane in dry state [44]. The void fraction, is thus calculated as:

$$\varphi_v = \left(\frac{W_{wet} - W_{dry}}{\rho_{water}} \right) + \frac{W_{dry}}{\rho_m} \quad (2)$$

The water content of the membranes was measured before and after every experimental run (all feed concentrations) until constant values, in order to verify that the gas permeation runs were conducted under constant humidity.

ATR-FTIR spectroscopy was performed using a Perkin Elmer spectrometer over 4 scans with a wave number resolution of 4 cm⁻¹ in the range 400–4000 cm⁻¹.

2.2. Gas Separation Experiments

The MMM composite membranes provide an effective membrane area of 15.6 cm². For the characterization of these membranes, they were placed in a stainless-steel module, which consists of two stainless steel pieces with a cavity where the membrane is placed using a 316LSS microporous disk support with a pore size of 20 μm and sealed by Viton Rings. Pure gas permeance of CH₄ and CO₂, in this order, was obtained using the home-made separation plant represented in Figure 2. The feed flow rate was set to 50 mL/min using mass flow controllers (KOFLOC 8500, Sequopro S.L., Madrid, Spain). The permeate flow rate was measured using a bubble flow meter at the exit of the membrane module. Feed pressure was set at 4 bar. Permeation experiments were run for 2 h for each pure gas, in order to ensure conditioning and steady state.

To carry on the validation of the model, different feed mixtures of CO₂/CH₄ were introduced to the system in relations of 35:65, 50:50, 20:80 and 70:30 v%, respectively, of each gas, being the possible biogas composition depending on the source. The permeate flow rate was measured at the exit of the entire system in the same way as pure gases, and to establish the composition of the permeate, a gas analyzer (BIOGAS5000, Geotech, Tamarac, FL, USA) was used. The experimental results of the permeate gas stream thus obtained for the PDMS commercial membrane were compared with the simulated results to validate the model described below.

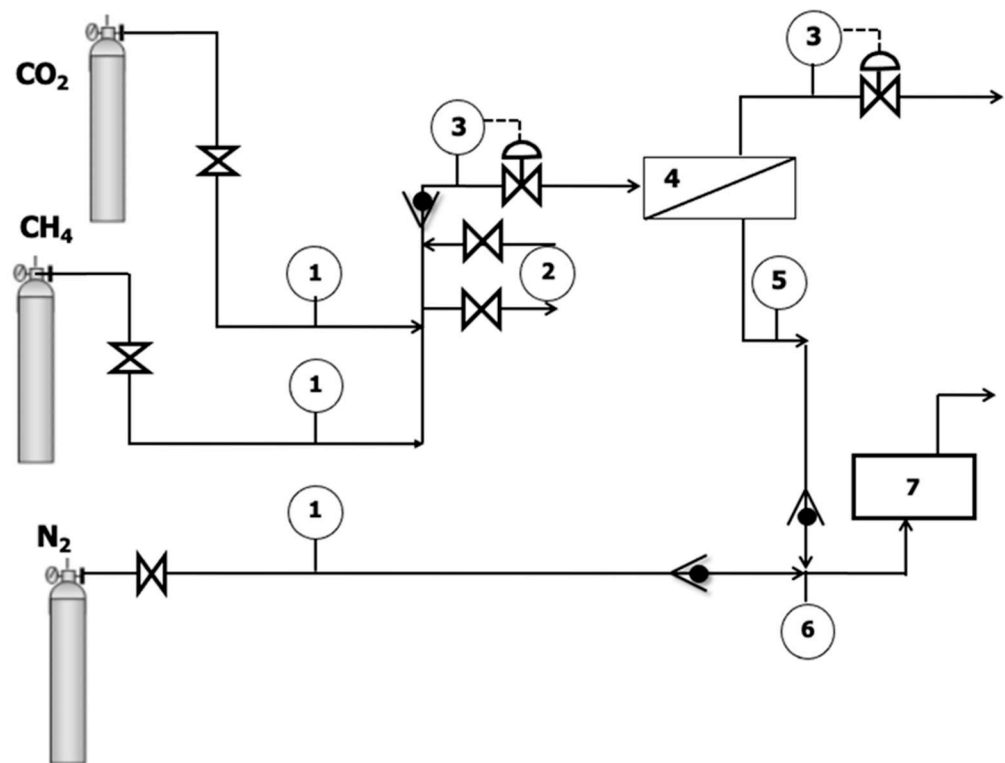


Figure 2. Experimental setup. (1) Mass flow controller, (2) Water bubbler, (3) Feed and retentate pressure regulator, (4) Membrane module, (5) Permeate pressure indicator, (6) Permeate flowmeter, (7) Gas analyzer.

The permeance of the gas I in units of GPU (1 GPU = 10^{-6} cm³ (STP) cm⁻² s⁻¹ cmHg⁻¹) is defined as the pressure-normalized flux of a gas through a membrane:

$$\left(\frac{P}{l}\right)_i = \frac{Q_p}{(p_r - p_p)A} \times 10^6 \tag{3}$$

where P is the intrinsic permeability of the selective membrane layer, in Barrer (1 barrer = 10^{-10} cm³ (STP) cm⁻¹ s⁻¹ cmHg⁻¹); p_r and p_p is the retentate and permeate pressure (bar), respectively; A is the effective area of the membrane (cm²); l is the selective layer thickness for the separation; Q_p is the permeate flow rate (cm³ (STP) s⁻¹) at measurement pressure and temperature conditions.

The selectivity of the membrane is defined by the ratio between the permeability of both pure gases across the membrane:

$$\alpha_{ij} = \frac{P_i}{P_j} \tag{4}$$

2.3. Process Simulation: Membrane Unit Model

A crossflow membrane model was built using Aspen Custom Modeler. For membrane modeling a tank in series model was applied where the membrane unit is divided in k number of equal sized uniform cells (being k variable from 1 to n), where the permeate of each cell is recovered and mixed with the rest of the permeate streams, the retentate of each cell being the feed for the next one, as represented in Figure 3 [52].

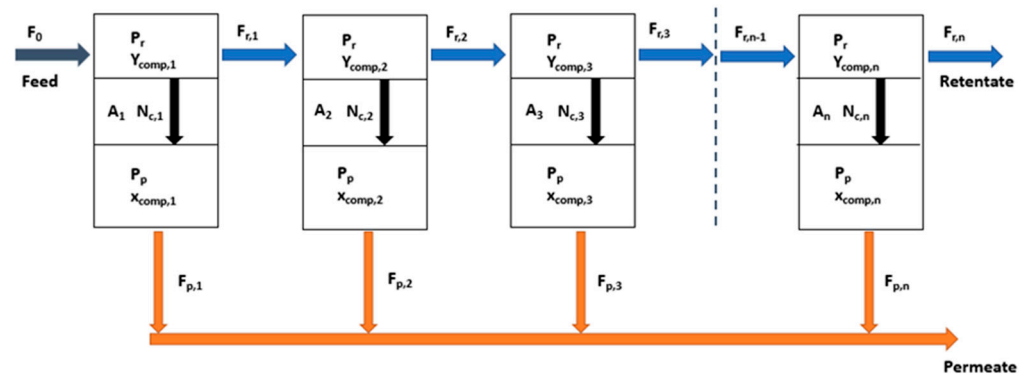


Figure 3. Diagram of the crossflow membrane model.

The main assumptions for this model in each cell are the following [53]:

- Ideal gas behavior.
- Isothermal and constant permeance.
- The pressure drop is negligible at each side of the membrane.
- The effect of concentration polarization is negligible.
- The permeance depends on the feed conditions and can be estimated based on correlations dependent on conditions, including pressure, flowrate, and composition.

According to the previous assumptions, steady state material balances were used to describe the changes in gas composition and flowrates at both sides of the membrane, whose expressions are shown in Equations (5)–(7) as follows.

For any k cell from 1 to n :

$$F_{r,k-1} = F_{r,k} + F_{p,k} \tag{5}$$

$$F_{r,k-1} y_{comp,k-1} = F_{r,k} y_{comp,k} + F_{p,k} x_{comp,k} \tag{6}$$

$$N_{comp,k} = F_{p,k} x_{comp,k} \tag{7}$$

In these equations, $F_{r,k}$ and $F_{p,k}$ are the total molar flowrate (kmol h^{-1}) of retentate and permeate leaving each cell respectively, $x_{comp,k}$ and $y_{comp,k}$ are the molar fraction of each component in the mixture present in the permeate and retentate streams and $N_{comp,k}$ is the molar flowrate of each component permeating through the membrane cell k (kmol h^{-1}) [53].

To describe the transport mechanism across the membrane the solution-diffusion model is used. In this model, the partial pressure difference across the membrane is the driving force of permeation [54]:

$$N_{comp,k} = A_k P_{comp} (p_r y_{comp,k} - p_p x_{comp,k}) \tag{8}$$

This is described by P_{comp} being the permeance for each component across the membrane converted to molar basis ($\text{kmol h}^{-1} \text{bar}^{-1} \text{m}^{-2}$, calculated from the experimentally obtained permeance in $\text{m}^3 \text{(STP) h}^{-1} \text{bar}^{-1} \text{m}^{-2}$ units), A_k is the membrane area of the cell k , and p_r and p_p are the pressure on the retentate and permeate sides of the membrane, respectively.

At the n th cell, outlet of the membrane, the retentate molar flowrate and the molar fraction of each component in this stream are the calculated for $k = n$, while the permeate molar flowrate of the outlet stream is obtained as the sum from $k = 1$ to n , and the corresponding molar fraction of components as follows:

$$F_{p,n} = \sum_{k=1,n} (F_{p,k}) \tag{9}$$

$$F_{p,n} \cdot x_{comp,n} = \sum_{k=1,n} (F_{p,k} x_{comp,k}) \tag{10}$$

The stage-cut is the ratio of the permeate flowrate to the feed flowrate, as shown in Equation (9) [55]:

$$\theta = F_p / F_f \quad (11)$$

To compare the separation performance of different membranes, two parameters are used: the purity and recovery of each component across the membrane, in:

$$\text{Purity}_{comp}(\%) = 100 \times \frac{F_{comp,out}}{F_{out}} = 100 \times \frac{F_{comp,out} y_{comp,out}}{F_{out}} = 100 \times y_{comp,out} \quad (12)$$

$$\text{Recovery}_{comp}(\%) = 100 \times \frac{F_{comp,out}}{F_{comp,in}} = 100 \times \frac{F_{out} y_{comp,out}}{F_{in} x_{comp,in}} \quad (13)$$

Both parameters are considered as the most important parameters to determine the effectiveness of the simulated membranes and all the specifications are focused on their values so that the optimization of the process aims at obtaining the maximum purities and recoveries of each component in the permeate for the most permeable one and on the retentate for the other. In response to the difficulty of maximizing both process parameters at the same time., a multi-objective problem would be proposed for establishing more global targets [56]. Another aspect that should be fixed before undertaking the simulation is the number of cells, n , required to achieve a determined objective. The magnitude of this process parameter determines the precision of the results obtained. In this work, we selected a value of $n = 100$ as a compromise between the numerical discretization and the model precision [56].

3. Results

3.1. Pure Gas Permeation Experiments

The results of single CO₂ and CH₄ permeation are plotted against the 2008 Robeson upper bound commonly used for comparing permselective membrane materials for a specific gas pair separation target, since it describes the trade-off of existing polymer materials to perform a certain gas pair separation [57]. Advancements on highly permeable advanced polymers and complex configurations, such as facilitated transport membranes, composite flat, and hollow fiber membranes, have led to revisions of these upper bound [58,59]. Several biopolymer MMM and composite membranes reported in literature [11] regarding this target separation are also included in Figure 4. The values are collected in Table A1 (Appendix A). The data points of the mixed matrix composite flat membranes evaluated in this work are encircled for comparison with literature.

A large number of fillers have been used in mixed matrix membranes for CO₂ separation. It is very important that the filler should have good compatibility with the polymer matrix to increase CO₂ separation performance, to avoid the formation of interfacial voids between the dispersed phase (fillers) and continuous matrices that imply a reduction in the CO₂ permselectivity of the membrane by allowing the transport of other species present in the feed through the voids [24]. Mixed matrix composite flat membranes made of thin layers of IL-CS loaded with nano-HKUST-1 observed an increase in CO₂ permeability and CO₂/CH₄ selectivity, attributed to the compatibility of the components in the MMM [44] that can be transferred to composite membranes when this MMM is coated on a compatible support [46]. This increase was even more apparent in wet conditions because of the high hydrophilicity of these material. The addition of two-dimensional fillers with higher aspect area/volume ratio as layered AM-4 [51] and UZAR-S3 [52] stannosilicate also seemed promising, although the permselectivity ratio is still low in thin composite form. This is attributed to the different hydrophilicity character of the material components [29,60]. The water uptake (Equation (1)) and dimensional swelling degree are calculated after Equations (1) and (2), respectively, and collected in Table 1. The water uptake is a measure of the hydrophilicity of the membrane and the dimensional swelling of the mechanical robustness upon performance. The porosity of the composite membranes studied in this work had an average value of $34 \pm 2\%$. The porosity (or void fraction) for the selective layer was

6 ± 2%. The average thickness of the selective layer was lower than 25 μm in the dry state. These results may support the evidence regarding the role of hydrophilicity on the CO₂ separation performance [61].

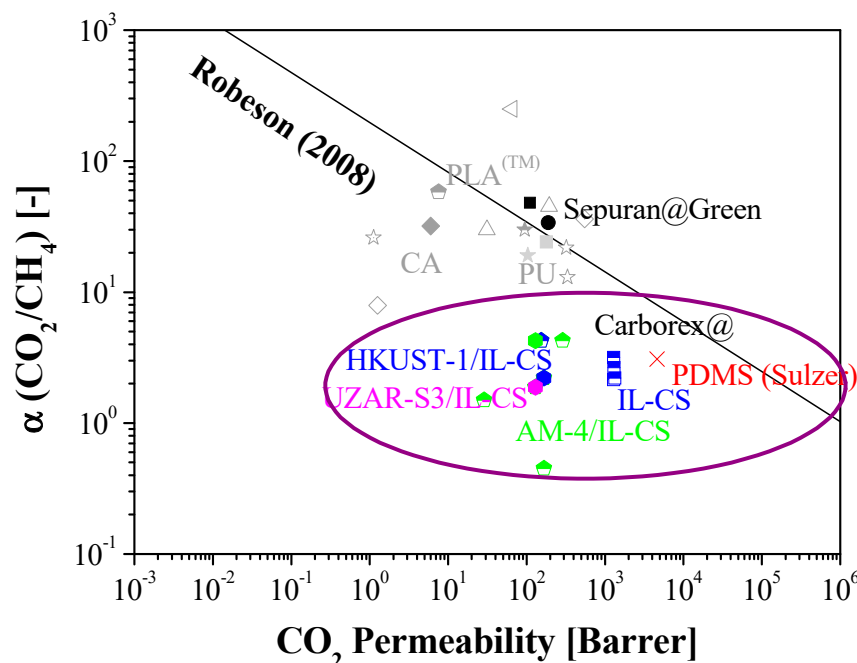


Figure 4. CO₂/CH₄ selectivity and CO₂ permeability of biopolymer-based mixed matrix and composite membranes against the 2008 Robeson upper bound [57]. Commercial membranes used for biogas separation are represented in grey and black for comparison. The values obtained in the single gas permeation experiments in this work are contained within the circle.

Table 1. Water Uptake and Swelling Degree calculation from measurements of dry and wet thickness and weight for the composite membranes studied in this work.

Membrane	Thickness (μm)		Weight (g)		WU (%)	SD (%)
	Dry	Wet	Dry	Wet		
PES	132		0.072			
IL:CS/PES (PDMS) ^a	151 ± 10	215 ± 50	0.225 ± 0.06	0.349 ± 0.052	55 ± 17	42 ± 27
IL:CS/PES (TMC) ^b	144 ± 4.4	237 ± 42	0.229 ± 0.028	0.341 ± 0.047	49 ± 12	64 ± 28
AM-4:IL-CS/PES	173 ± 22	222 ± 15	0.137 ± 0.004	0.223 ± 0.015	63 ± 9.4	28 ± 9.1
UZAR-S3:IL-CS/PES	174 ± 0.1	194 ± 4.9	0.136 ± 0.002	0.209 ± 0.007	54 ± 2.8	11 ± 2.4
HKUST-1:IL-CS/PES	180 ± 2.8	214 ± 6.3	0.134 ± 0.007	0.256 ± 0.006	90 ± 5.3	19 ± 1.7

^a IL:CS coating prepared over a PDMS gutter layer over the microporous PES support; ^b IL:CS coating prepared by the modified interfacial polymerization method as reported elsewhere [46].

The ATR-FTIR spectra of dry IL-CS/PES composite membranes are shown in Figure 5. The analyses were performed after the gas permeation runs and drying to constant weight in order to avoid the masking of the intrinsic peaks of the selective layer materials by the abundant presence of hydroxyl groups due to the water adsorbed in them [62]. The intensity appears to be independent of the type of filler in the IL-CS matrix. The bands of the MMM layer do not shift from the IL-CS spectra, thus implying that the interaction between the filler and the continuous matrix is good and homogeneously dispersed as studied in previous works upon the self-standing films [63].

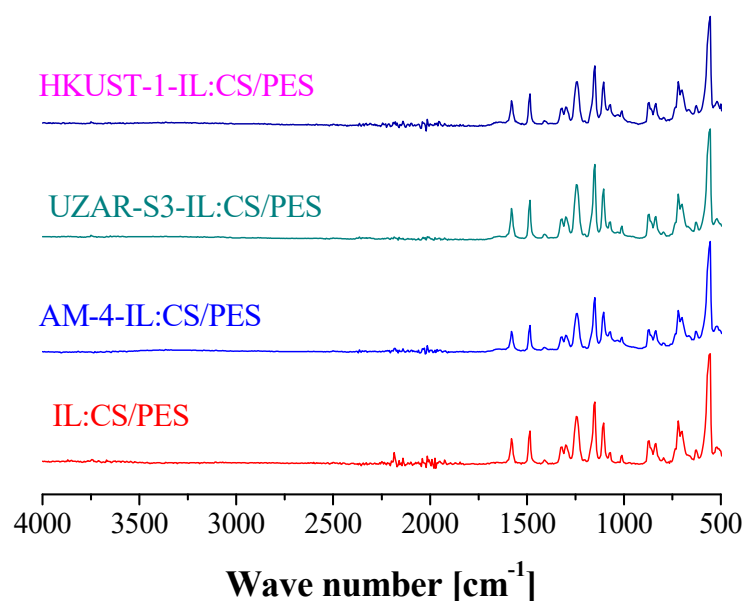


Figure 5. ATR-FTIR spectra of the IL:CS/PES based composite membranes as a function of MMM layer composition.

3.2. Process Simulation and Sensitivity Analyses

3.2.1. Model Validation

For the membrane cell modeling, the experimental process conditions as well as the membrane parameters, in terms of selectivity and permeability, were required for the simulation task in order to evaluate the process performance in terms of purity and recovery of CO₂ at the permeate side, which were used for the model validation, and the corresponding parameters of CH₄ in the retentate side. This validation was made with a PDMS commercial membrane, which provided a single CO₂ gas permeance value of 369.29 GPU and a CO₂/CH₄ selectivity of 3.11 (Equation (4)). The experimental results obtained for the separation of CO₂/CH₄ gas mixtures using a commercial PDMS membrane were used to validate the model Equations (12) and (13), for the target objectives of purity and recovery, respectively. The simulated values of the CO₂ permeate purity and recovery were determined by introducing the experimental CO₂ permeance and CO₂/CH₄ selectivity at each feed composition, as well as the experimental stage-cut, into the developed model. Figure 6 compares those CO₂ permeate purity and recovery experimental (black) and simulated (red) values (%) as a function of the feed gas mixture. The model is validated by the experimental results of the separation of CO₂/CH₄ mixtures with the commercial PDMS membrane.

The deviation between the experimental and simulated results was estimated as an absolute relative error, AARE, using Equation (14). The values obtained for the CO₂ and CH₄ permeate purity and recovery using the commercial PDMS membrane as reference, are collected in Tables A2 and A3 and by applying material balances, Tables A4 and A5 represent the retentate purity and recovery, respectively (Appendix A). Except for the experiment of CO₂/CH₄ 30:70 v% feed, which corresponded to AARE values for the CH₄ component around 25%, the AARE values obtained for the PDMS reference membrane validate the model within acceptable range (below 20% and significantly lower values):

$$\text{AARE} = 100 \times \left| \frac{\text{Simulated Value} - \text{Experimental Value}}{\text{Experimental Value}} \right|, \quad (14)$$

Considering the results obtained for the experimental and the simulation studies, if we consider the existence of an experimental error when obtaining the mean value of the two parameters represented with their standard deviation, it can be stated that the fit of

the model is adequate to describe the performance of the membranes characterized by its permeability and selectivity.

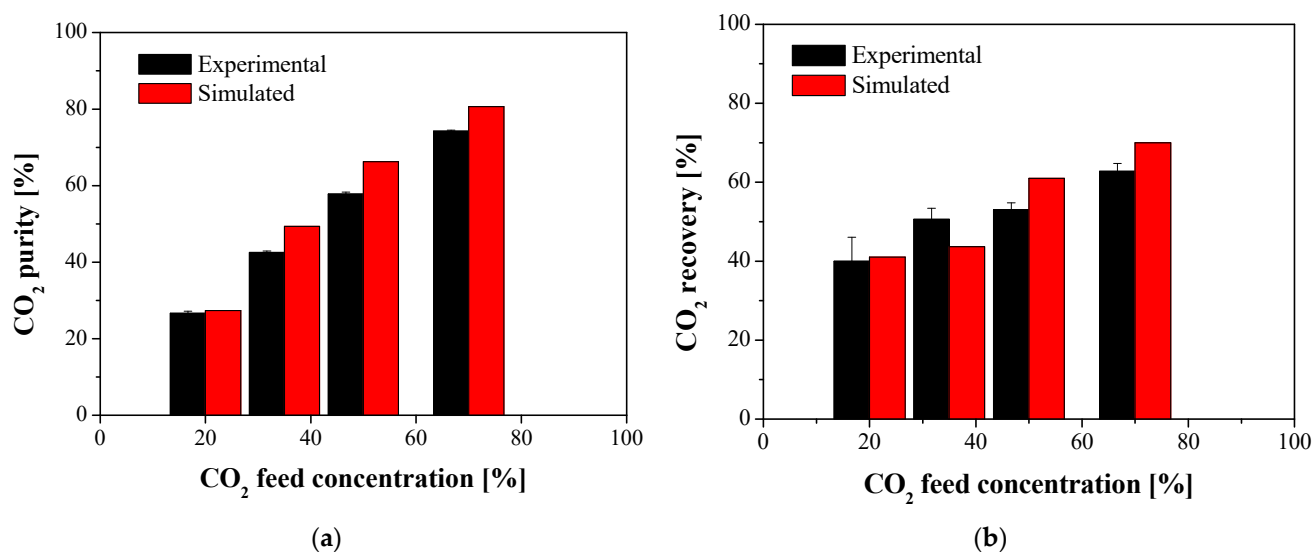


Figure 6. Experimental and simulated CO₂ permeate purity (a) and recovery (b) as a function of CO₂ feed concentrations for a PDMS commercial membrane. (Temperature = 20 °C, feed pressure = 4 bar).

3.2.2. Influence of Feed Concentration

The experimental results were used to validate the developed mathematical model. The CO₂/CH₄ gas mixture separation of the chitosan based composite membranes was thus compared with the reference commercial PDMS membrane. Figure 7 shows the results of the simulations of the permeate purity and recovery selected as target objective variables as a function of CO₂ concentration in the feed. The stage-cut and feed pressure considered for the modelling equations were 0.5 and 4 bar, respectively, in agreement with the experimentally obtained values. The CO₂ purity in the permeate increases while the recovery decreases with increasing CO₂ concentration in the feed, which indicates that some CO₂ goes to the retentate, decreasing the recovery of the CH₄ in the retentate [56]. All the membranes observe a similar trend and IL-CS and AM-4:IL-CS composite membranes provide the largest values of CO₂ and CH₄ purity, closely followed by the commercial PDMS membrane. The purity values of IL-CS and AM-4:IL-CS composite membranes reached a CO₂ purity of 88% at high CO₂ concentration in the feed and a maximum recovery of around 82% against the 84% CO₂ purity and maximum recovery of 75% from simulation with the commercial membrane. The CO₂ purity and recovery with UZAR-S3:IL-CS and HKUST-1:IL-CS composite membranes are 80% and 75%, respectively. As expected, the performance of CH₄ purity and recovery is the opposite with increasing CO₂ concentration in the feed. CH₄ purity is reduced from 88.9% to 48% for the CS-IL and AM-4: IL-CS composite membranes, and from 89% to 40% for the other IL-CS-based composite membranes. The recovery of CH₄ increases 10% for the UZAR-S3- and HKUST-1: IL-CS membranes, against 20% for the PDMS commercial membrane, whereas AM-4:IL-CS composite membrane observed a CH₄ recovery up to 30%. The best behavior in CO₂/CH₄ separation and recovery is thus related to the hydrophilic character of both the CS-based matrix and the AM-4 filler, since hydrophilicity has been observed to facilitate the transport through water-swollen composite membranes [29]. The AM-4 filler is also more easily dispersed than UZAR-S3 and HKUST-1 in the CS matrix [46,49] and provides additional CO₂ adsorptive properties [50] to the membrane when embedded in the IL-CS matrix of the selective layer of the membrane. These results give scope for the possibility of substitution of PDMS by renewable materials.

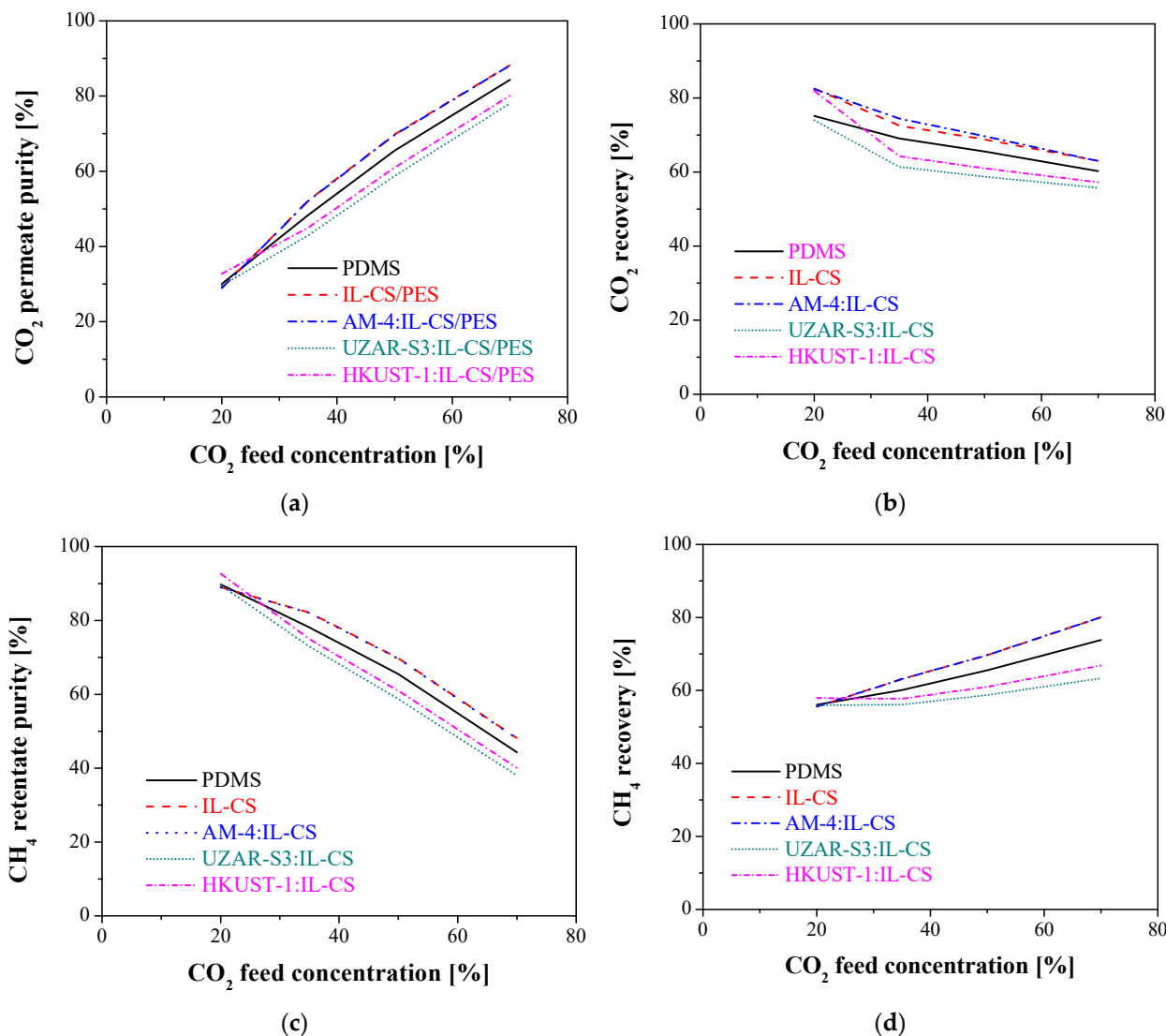


Figure 7. Influence of the CO₂ feed concentration in (a) CO₂ purity in the permeate, (b) CO₂ recovery, (c) CH₄ purity in the retentate, and (d) CH₄ recovery for all the membranes tested in this work at the experimental stage-cut of 0.5 and a feed pressure of 4 bar.

According to these results, variations in the feed concentration have a stronger impact on the purity than in the recovery of both components in the outlet streams.

3.2.3. Influence of the Stage-Cut

A sensitivity analysis to study the capacity of the synthesized membranes via the stage-cut variable is presented below, at a fixed feed concentration of 65% of CH₄, 35% of CO₂, simulating the base raw biogas concentration without the trace components (hydrogen sulfide, water vapor, ammonia, and siloxane) that may be present depending on the types of feedstock and digestion process [63]. Different values of stage-cut, ranging from 0.1 to 0.9, were considered to calculate the evolution of purity and recovery of CH₄ in the retentate and CO₂ in the permeate, which are plotted in Figure 8.

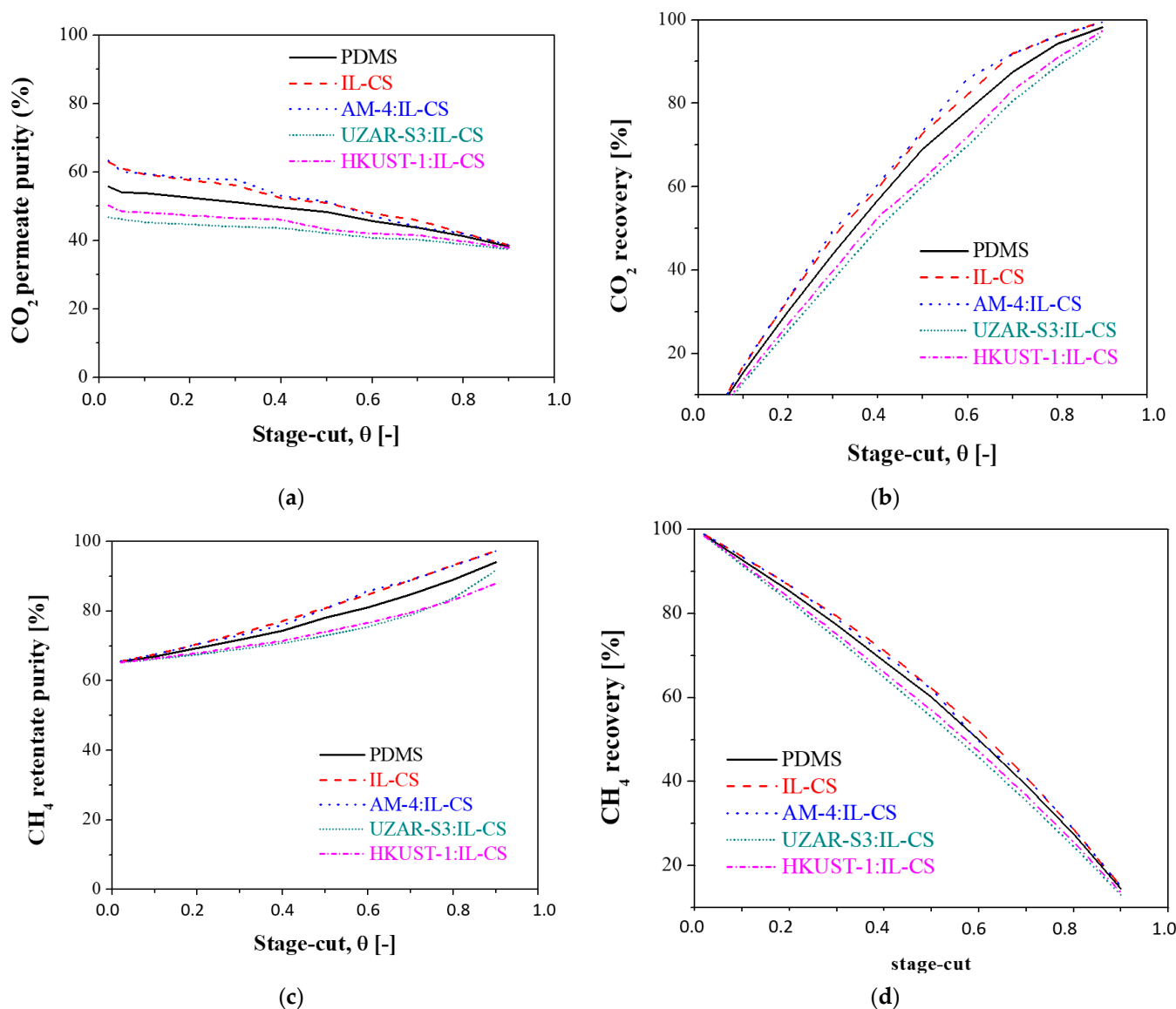


Figure 8. Influence of the stage-cut for the membranes tested in this work on: (a) the CO₂ purity in the permeate, (b) the CO₂ recovery in the permeate, (c) the CH₄ purity in the retentate, and (d) the CH₄ recovery in the retentate. Feed concentration: 35% CO₂: 65% CH₄, feed pressure: 4 bar.

In Figure 8, an increase in the CH₄ purity in the retentate and the CO₂ recovery in the permeate are observed with increasing stage-cut. While a high value of stage-cut is needed to attain a CO₂ recovery close to 100%, the CO₂ purity of all the membranes tested in this work was below 65% in all the range of stage-cut studied. This confirms the compromise between these target objective parameters. The increase in CH₄ purity in the retentate with increasing stage-cut is lower than that of CO₂ purity, from an initial 66% to a final 94% for the commercial PDMS, 91.7% for the UZAR-S3:IL-CS membrane, and 87.9% for the HKUST-1:IL-CS membranes. Again, IL-CS and AM-4:IL-CS membranes reached the highest CH₄ purities of 97.2%. The reduction in CO₂ purity with increasing stage-cut ratio is related to methane losses in the permeate stream due to the higher amount of gas passing through the membrane. This explains the reduction in CH₄ recovery in the retentate, going from 92.8%, 93.6%, 93.5%, 91.5% and 91.9%, to 14.5%, 15%, 15%, 12.9% and 13.5% for PDMS, IL-CS, AM-4:IL-CS, UZAR-S3:IL-CS and HKUST-1:IL-CS composite membranes, respectively, when stage-cut increases from 0.1 to 0.9. The CO₂ recovery would be drastically increased from around 15% to 98.3% for PDMS, 99.5% for the IL-CS and AM-4:IL-CS, 96.2% and 97.4% for the UZAR-S3:IL-CS and HKUST-1:IL-CS composite membranes, respectively. These results

give evidence again of the significance of hydrophilicity and CO₂ adsorptive properties of the components of the top layer of the composite membrane upon CO₂ separation [64].

The relationship between the stage-cut and the required total membrane area is plotted in Figure 9. As expected, higher stage-cut values require a larger membrane area. The membrane area required for the PDMS commercial membrane is included for comparison, although the value is ten-fold less than the IL-CS-based composite membranes because of the higher experimental permeation rate.

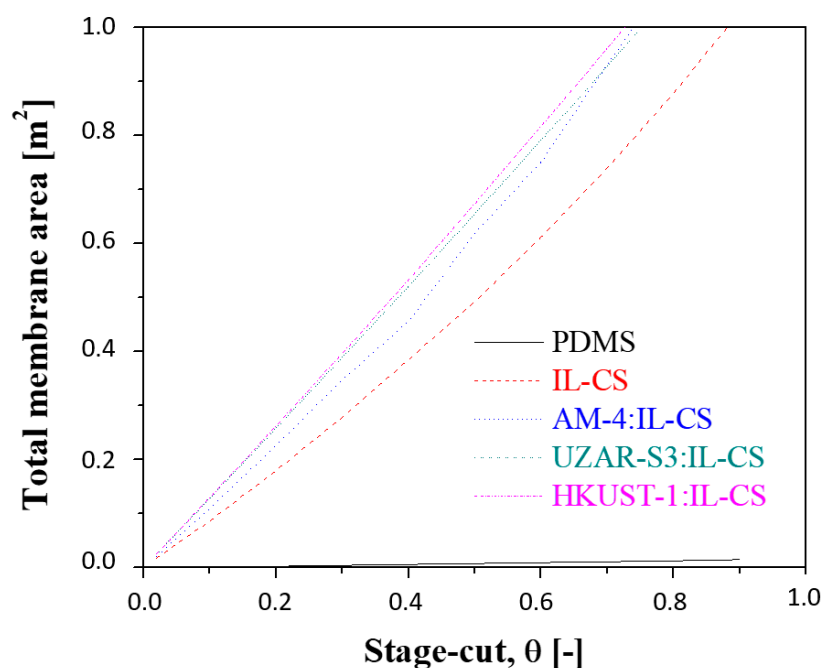


Figure 9. Evolution of the required membrane area as a function of stage-cut. Experimental feed flow rate: 50 mL/min, feed pressure: 4 bar. Feed concentration: 35% CO₂: 65% CH₄.

3.3. Comparison with Literature

Membranes prepared with three other type of biopolymers were selected from the literature to be compared with the membranes presented in this study regarding the target objectives and CO₂/CH₄ separation performance. These membranes were selected on account of the different values of CO₂ permeance and CO₂/CH₄ selectivity to check the applicability of the model to membranes in a wider range of membrane properties. These membranes are a CA hollow fiber membrane with a CO₂ permeance of 248 GPU and a CO₂/CH₄ selectivity of 7.9 [65], a ZIF-8:CS/PES composite membrane with CO₂ permeance of 26.6 GPU and a selectivity of 24.2 [40], and a CNT:PVAm-PVA/PSf composite membrane with a CO₂ permeance of 129 GPU and a CO₂/CH₄ selectivity of 45 [30]. The simulations were run by varying the stage-cut in the range from 0.1 to 0.9 and the results are shown in Figures 10 and 11 for CO₂ and CH₄, respectively.

Firstly, Figure 10 considers the results obtained at the permeate side, for CO₂, observing the process performance, since an increase in CO₂ recovery implies a decrease in CO₂ purity, as more CO₂ goes through the membrane to the permeate but the permeate quality is lower with increasing stage-cut. The PVAm-PVA based membrane provides a purity of 89%, followed by the grafted ZIF-8:CS composite membrane, with a purity of 82.5% and the CA hollow fiber membrane a CO₂ purity of 69%, which is closer to the membranes prepared in this work. On the other hand, all the membranes analyzed reached a CO₂ recovery higher than 99%, at high values of stage-cut. These results provide evidence of the possibility of using green alternative materials to fabricate membranes with similar performance as other membranes.

Figure 11 shows the trade-off for CH₄ purity and recovery in the retentate. As before, when purity increases, recovery decreases, but in this case, the results provided for our membranes are in the same order of magnitude as those of the literature membranes. IL-CS and AM-4:IL-CS composite membranes could achieve a purity of 97.2%, very close to the literature ones.

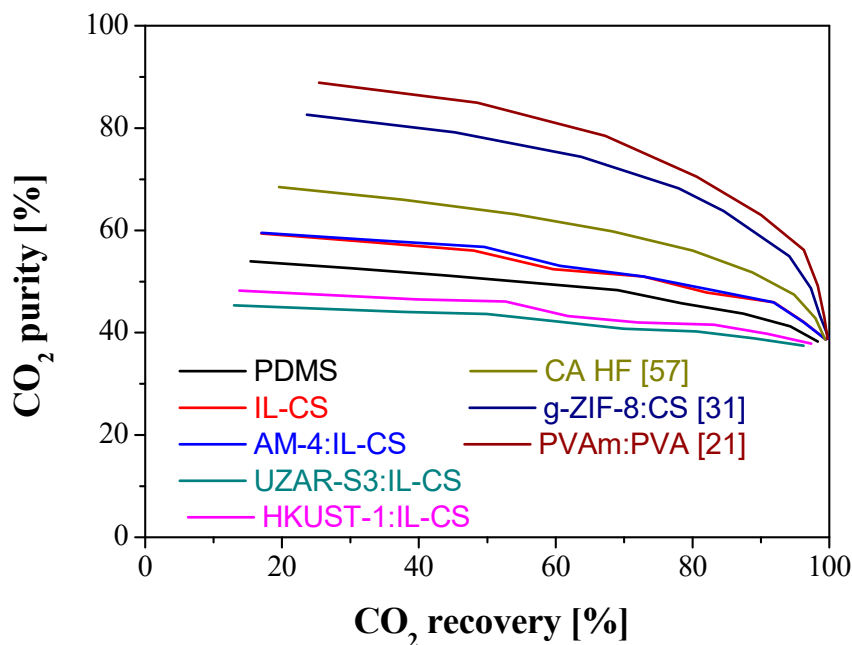


Figure 10. Comparison of the results of CO₂ purity versus CO₂ recovery in the permeate for the membranes prepared in this study with the three biopolymer-based membranes selected from the literature. Feed concentration: 35% CO₂: 65% CH₄. Feed pressure: 4 bar. Feed flow rate: 50 mL/min.

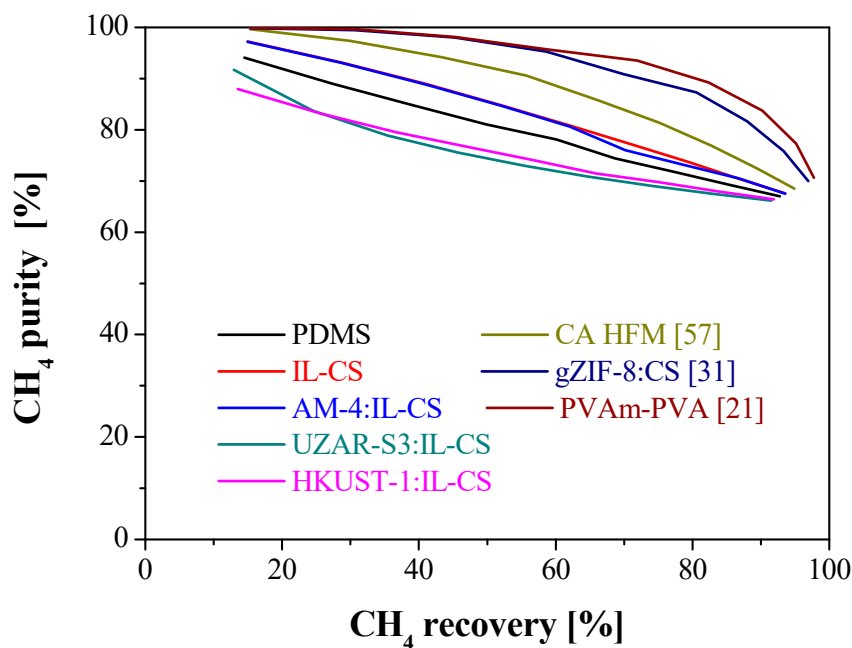


Figure 11. Comparison of the results of CH₄ purity versus CH₄ recovery in the retentate for the prepared membranes in this study with three selected membranes based on biopolymers from the literature. Feed concentration: 35% CO₂: 65% CH₄. Feed pressure: 4 bar. Feed flow rate: 50 mL/min.

4. Conclusions

Membrane technology is considered as a sustainable technology for biogas purification, but the membrane materials used for the fabrication of commercial membranes are still based on fossil fuels and costly reactants and solvents, thus biopolymer-based membranes are being studied as a green alternative for CO₂/CH₄ separation. In this work, composite membranes made of chitosan matrix hybridized by [emim][acetate] IL and different nano-porous fillers previously studied in our laboratory: CO₂-sorptive AM-4 layered titanosilicate, nanoporous UZAR-S3 lamellar stannosilicate and nanometric sized HKUST-1. The CO₂/CH₄ performance of the mixed matrix composite membranes was evaluated experimentally in single gas and gas mixture CO₂/CH₄ mode separation. Although the permeance and selectivity are still below commercial membranes and further work is being carried out to increase performance of these chitosan-based membranes, the hydrophilic and compatibility factor of the membrane components seem to play a significant role in facilitating the transport of CO₂ across the membrane and influencing the purity and recovery of both gases in the permeate and retentate, respectively.

Besides, in this work a mathematical model was applied to the CO₂/CH₄ separation with different types of bio-based membranes. The model was first validated using a commercial PDMS membrane and then the chitosan-based composite membrane performance was analyzed in terms of the target objectives of CO₂ and CH₄ recovery and purity in the permeate and retentate, respectively. The IL-CS and AM-4:IL-CS composite membranes, of higher hydrophilic and CO₂ adsorptive character, showed the most promising results, close or even surpassing those of the hydrophobic commercial membrane used as reference. This provides scope for alternative membrane materials fabricated from renewable or bio-degradable polymers and non-toxic fillers to show at least comparable CO₂/CH₄ separation as existing membranes, as well as the simultaneous feedback on membrane development enabled by the simultaneous correlation of the process requirements with the membrane properties to achieve those process targets by the simulation and optimization tools supporting the experimental work.

Author Contributions: Conceptualization and methodology, C.C.-C. and A.G.; software, A.G.; validation, A.T.-C.; investigation, C.C.-C.; resources, A.G.; data curation, A.T.-C.; writing—original draft preparation, A.T.-C.; writing—review and editing, C.C.-C.; supervision, C.C.-C. and A.G.; project administration, A.G. All authors have read and agreed to the published version of the manuscript.

Funding: This research was funded by the Spanish Ministry of Science and Innovation, grant number PID2019-108136RB-C31/AEI/10.13039/501100011033, and European Union Next Generation EU/PRTR, grant number EIN2020-112319/AEI/10.13039/501100011033. The Spanish Ministry of Science and Innovation is also gratefully acknowledged for grant PRE2020-09765/AEI/10.13039/501100011033 (A.T.C.). The APC is funded by the University of Cantabria.

Institutional Review Board Statement: Not applicable.

Data Availability Statement: Not applicable.

Acknowledgments: Ricardo Abejón from the University of Santiago de Chile is thanked for his efforts on the mathematical model development for simulation and optimization of membrane separation processes.

Conflicts of Interest: The authors declare no conflict of interest.

Nomenclature

Symbol	Description
AM-4	Layered titanosilicate
A	Membrane area (cm ²)
Barrer	Unit of permeability (1 barrer = 10 ⁻¹⁰ cm ³ (STP) cm ⁻¹ s ⁻¹ cmHg ⁻¹)
CA	Cellulose acetate
CH ₄	Methane

CNC	Crystalline nanocellulose
CNTs	Carbon nanotubes
CO ₂	Carbon dioxide
CS	Chitosan
[emim][Ac]	1-ethyl-3-methylimidazolium [emim][Ac]
$F_{r,k}$	Total molar flowrate of retentate (kmol h ⁻¹) in cell k
$F_{p,k}$	Total molar flowrate of permeate (kmol h ⁻¹) in cell k
GPU	Unit of permeance (1 GPU = 10 ⁻⁶ cm ³ (STP) cm ⁻² s ⁻¹ cmHg ⁻¹)
HKUST-1	Metal organic framework (MOF)
IL	Ionic liquid
l	Selective layer thickness for the separation (mm)
MMM	Mixed matrix membrane
$N_{comp,k}$	Molar flowrate of each component permeating through the membrane cell k (kmol h ⁻¹)
NaOH	Sodium hydroxide
Na ₂ SiO ₃	Sodium silicate
Nps	Nanoparticles
P	Permeability of the selective membrane layer (Barrer)
p_r	Retentate pressure (bar)
p_p	Permeate pressure (bar)
PDMS	Polydimethyl siloxane
PEG	Polyethylene glycol
PES	Polyethersulfone
PSf	Polysulfone
PU	Polyurethane
PVA	Polyvinyl alcohol
PVAm	Polyvinyl amine
Q_p	Permeate flow rate (cm ³ (STP) s ⁻¹)
SnCl ₂ · 2H ₂ O	Tin(II) chloride di-hydrated
TiO ₂	Anatase
TMC	Trimesoyl chloride
UZAR-S3	Layered stannosilicate
α_{ij}	Selectivity of component i over j
$x_{comp,k}$	Molar fraction of each component in the permeate
$y_{comp,k}$	Molar fraction of each component in the retentate

Appendix A

Table A1. Comparison of selected biopolymer-based membranes for CO₂/CH₄ separation with the membranes evaluated in this work.

Membrane ¹	Selective Layer Thickness [μm]	CO ₂ Permeability [Barrer]	CO ₂ /CH ₄ Selectivity [-]	Reference
CA (18 wt%) HF	50	1.26	7.9	[66]
CNT (1 wt%)/CA (3 wt%)	35	14.2	21.2	[67]
NH ₂ -MIL-53(Al) (15 wt%)/CA (10 wt%)		52.6	28.7	[68]
PVAm-PVA blend	0.6	31.2	30	[29,65]
CNC/PVA	0.8	86	43	[31]
CNT (1 wt%)/PVAm-PVA	1.5	129	45	[30]
NiO (5 wt%)/PU (10 wt%)	100	321	21.76	[32]
IL-PEG-PU	97.5	499	44	[33]
SAPO-34 (20 wt%)/PU (3 wt%)	65	28.71	25.63	[35]
CS-gC ₃ N ₄ -ZIF-8/PES	20	180	24.2	[40]
IL-CS/PES	14	1024	16	[47]
HKUST-1(5 wt%)-IL-CS/PES	67	26,872	30	[47]
IL-CS/PES	22.4	154 ± 18	4.26	This work

Table A1. *Cont.*

Membrane ¹	Selective Layer Thickness [μm]	CO ₂ Permeability [Barrer]	CO ₂ /CH ₄ Selectivity [-]	Reference
AM-4:IL-CS/PES	52.5	287 \pm 132	4.25	This work
UZAR-S3:IL-CS/PES	42.5	129 \pm 19	1.88	This work
HKUST-1-IL-CS/PES	50.4	167 \pm 32	2.21	This work

¹ PU: polyurethane; PVAm: polyvinyl acetylamine; PVA: polyvinyl alcohol; CS: chitosan; gC₃N₄ grafted carbon nitride; pes: polyether sulfone support; CNT: carbon nanotubes; CA cellulose acetate; CNC: semicrystals of nanocellulose.

Table A2. Experimental CO₂ permeate purity and recovery as a function of CO₂ concentration in the feed and experimental stage-cut for the commercial PDMS membrane. The error of the model validation calculated by Equation (14) is given in the last columns.

CO ₂ in Feed (v%)	Stage-Cut	CO ₂ Purity in Permeate (%)	CO ₂ Recovery (%)	AARE _{purity} (%)	AARE _{recovery} (%)
20	0.30	26.67 \pm 0.5	39.98 \pm 6.08	2.60	2.67
35	0.31	42.55 \pm 0.36	50.60 \pm 2.76	16.02	13.59
50	0.46	57.81 \pm 0.52	52.99 \pm 1.80	14.63	15.06
70	0.59	74.24 \pm 0.24	62.76 \pm 1.82	8.62	8.31

Table A3. Experimental CH₄ permeate purity and recovery as a function of CH₄ concentration in the feed and experimental stage-cut for the commercial PDMS membrane. The error of the model validation calculated by Equation (14) is given in the last columns.

CH ₄ in Feed (v%)	Stage-Cut	CH ₄ Purity in Permeate (%)	CH ₄ Recovery (%)	AARE _{purity} (%)	AARE _{recovery} (%)
30	0.59	25.75 \pm 0.28	50.79 \pm 1.47	24.84	25.05
50	0.46	42.19 \pm 0.52	38.68 \pm 1.65	20.05	19.77
65	0.31	57.44 \pm 0.36	27.25 \pm 1.49	11.87	12.86
80	0.30	72.64 \pm 0.27	30.49 \pm 4.39	0.95	10.67

Table A4. Experimental CO₂ retentate purity and recovery as a function of CO₂ concentration in the feed and experimental stage-cut for the commercial PDMS membrane. The error of the model validation calculated by Equation (14) is given in the last columns.

CO ₂ in Feed (v%)	Stage-Cut	CO ₂ Purity in Retentate (%)	CO ₂ Recovery (%)	AARE _{purity} (%)	AARE _{recovery} (%)
20	0.30	17.11 \pm 0.63	60.02 \pm 6.10	1.82	1.99
35	0.31	31.63 \pm 0.31	62.51 \pm 2.04	9.54	9.77
50	0.46	43.39 \pm 0.50	47.01 \pm 1.81	16.71	16.97
70	0.59	63.83 \pm 0.24	37.24 \pm 1.82	14.46	14.13

Table A5. Experimental CH₄ retentate purity and recovery as a function of CH₄ concentration in the feed and experimental stage-cut for the commercial PDMS membrane. The error of the model validation calculated by Equation (14) is given in the last columns.

CH ₄ in Feed (v%)	Stage-Cut	CH ₄ Purity in Retentate (%)	CH ₄ Recovery (%)	AARE _{purity} (%)	AARE _{recovery} (%)
30	0.59	36.17 \pm 0.62	49.21 \pm 1.47	25.52	26.07
50	0.46	56.61 \pm 0.50	61.32 \pm 1.65	12.81	12.47
65	0.31	68.37 \pm 0.30	72.75 \pm 1.49	4.41	4.00
80	0.30	82.88 \pm 0.63	72.49 \pm 4.39	0.38	0.41

References

1. NOAA. Trends in Atmospheric Carbon Dioxide, (n.d.). 24 March 2022. Available online: <https://gml.noaa.gov/ccgg/trends/data.html> (accessed on 24 March 2022).
2. Keairns, D.L.; Darton, R.C.; Irabien, A. The Energy-Water-Food nexus. *Annu. Rev. Chem. Biomol. Eng.* **2016**, *7*, 239–262. [[CrossRef](#)] [[PubMed](#)]
3. He, Y.; Bagley, D.M.; Leung, K.T.; Liss, S.N.; Liao, B.Q. Recent advances in membrane technologies for biorefining and bioenergy production. *Biotechnol. Adv.* **2012**, *30*, 817–858. [[CrossRef](#)] [[PubMed](#)]
4. Persson, M.; Jonsson, O.; Wellinger, A. Biogas Upgrading to Vehicle Fuel Standards and Grid. *IEA Bioenergy* **2007**, *37*, 1–32.
5. Awe, O.W.; Zhao, Y.; Nzihou, A.; Minh, D.P.; Lyczko, N. A Review of Biogas Utilisation, Purification and Upgrading Technologies. *Waste Biomass Valorization* **2017**, *8*, 267–283. [[CrossRef](#)]
6. Rasi, S.; Lantela, J.; Rintala, J. Trace compounds affecting biogas energy utilization—A review. *Energy Convers. Manag.* **2011**, *52*, 3369–3375. [[CrossRef](#)]
7. Baciocchi, R.; Carnevale, E.; Costa, G.; Gavasci, R.; Lombardi, L.; Olivieri, T.; Zanchi, L.; Zingaretti, D. Performance of a biogas upgrading process based on alkali absorption with regeneration using air pollution control residues. *Waste Manag.* **2013**, *33*, 2694–2705. [[CrossRef](#)]
8. Scholz, M.; Melin, T.; Wessling, M. Transforming biogas into biomethane using membrane technology. *Renew. Sustain. Energy Rev.* **2013**, *17*, 199–212. [[CrossRef](#)]
9. Merkel, T.C.; Lin, H.; Wei, X.; Baker, R. Power plant post-combustion carbon dioxide capture: An opportunity for membranes. *J. Membr. Sci.* **2010**, *359*, 126–139. [[CrossRef](#)]
10. Lin, H.; Daniels, R.; Thompson, S.M.; Amo, K.D.; He, Z.; Merkel, T.C.; Wijmans, J.G. Membrane selective exchange process for dilute methane recovery. *J. Membr. Sci.* **2014**, *469*, 11–18. [[CrossRef](#)]
11. Russo, F.; Galiano, F.; Iulianelli, A.; Basile, A.; Figoli, A. Biopolymers for sustainable membranes in CO₂ separation: A review. *Fuel Process. Technol.* **2021**, *213*, 106643. [[CrossRef](#)]
12. Jusoh, N.; Keng, L.K.; Shariff, A.M. Preparation and characterization of polysulfone membrane for gas separation. *Adv. Mater. Res.* **2014**, *917*, 307–316. [[CrossRef](#)]
13. Wind, J.D.; Sirard, S.M.; Paul, D.R.; Green, P.F.; Johnston, K.P.; Koros, W.J. Carbon dioxide-induced plasticization of polyimide membranes: Pseudo-equilibrium relationships of diffusion, sorption, and swelling. *Macromolecules* **2003**, *36*, 6433–6441. [[CrossRef](#)]
14. Vu, D.Q.; Koros, W.J.; Miller, S.J. Mixed matrix membranes using carbon molecular sieves I. Preparation and experimental results. *J. Membr. Sci.* **2003**, *211*, 311–334. [[CrossRef](#)]
15. Larocca, N.M.; Pessan, L.A. Effect of antiplasticisation on the volumetric, gas sorption and transport properties of polyetherimide. *J. Membr. Sci.* **2003**, *218*, 69–92. [[CrossRef](#)]
16. Iqbal, M.; Man, Z.; Mukhtar, H.; Dutta, B.K. Solvent effect on morphology and CO₂/CH₄ separation performance of asymmetric polycarbonate membranes. *J. Membr. Sci.* **2008**, *318*, 167–175. [[CrossRef](#)]
17. Sridhar, S.; Aminabhavi, T.M.; Ramakrishna, M. Separation of binary mixtures of carbon dioxide and methane through sulfonated polycarbonate membranes. *J. Appl. Polym. Sci.* **2007**, *105*, 1749–1756. [[CrossRef](#)]
18. Kamble, A.R.; Patel, C.M.; Murthy, Z.V.P. Polyethersulfone based MMMs with 2D materials and ionic liquid for CO₂, N₂ and CH₄ separation. *J. Environ. Manag.* **2020**, *262*, 110256. [[CrossRef](#)]
19. Bui, M.; Adjiman, C.S.; Bardow, A.; Anthony, E.J.; Boston, A.; Brown, S.; Fennell, P.S.; Fuss, S.; Galindo, A.; Hackett, L.A.; et al. Carbon capture and storage (CCS): The way forward. *Energy Environ. Sci.* **2018**, *11*, 1062–1176. [[CrossRef](#)]
20. Gascon, J.; Kapteijn, F.; Zornoza, B.; Sebastian, V.; Casado, C.; Coronas, J. Practical approach to zeolitic membranes and coatings: State of the art, opportunities, barriers, and future perspectives. *Chem. Mater.* **2012**, *24*, 2829–2844. [[CrossRef](#)]
21. Brinkmann, T.; Lilleparg, J.; Notzke, H.; Pohlmann, J.; Shishatskiy, S.; Wind, J.; Wolff, T. Development of CO₂ selective poly(ethylene oxide)-based membranes: From laboratory to pilot plant scale. *Engineering* **2017**, *3*, 485–493. [[CrossRef](#)]
22. Kai, T.; Kouketsu, T.; Duan, S.; Kazama, S.; Yamada, K. Development of commercial-sized dendrimer composite membrane modules for CO₂ removal from flue gas. *Sep. Purif. Technol.* **2008**, *63*, 524–530. [[CrossRef](#)]
23. Castro-Munoz, R.; Gonzalez-Valdez, J. New trends in biopolymer-based membranes for pervaporation. *Molecules* **2019**, *24*, 3584. [[CrossRef](#)] [[PubMed](#)]
24. Borgohain, R.; Pattnaik, U.; Prasad, B.; Mandal, B. A review on chitosan-based membranes for sustainable CO₂ separation applications: Mechanism, issues, and the way forward. *Carbohydr. Polym.* **2021**, *267*, 118178. [[CrossRef](#)]
25. Moghadassi, A.R.; Rajabi, Z.; Hosseini, S.M.; Mohammadi, M. Fabrication and modification of cellulose acetate based mixed matrix membrane: Gas separation and physical properties. *J. Ind. Eng. Chem.* **2014**, *20*, 1050–1060. [[CrossRef](#)]
26. Mubashir, M.; Yeong, Y.F.; Lau, K.K.; Chew, T.L.; Norwahyu, J. Efficient CO₂/N₂ and CO₂/CH₄ separation using NH₂-MIL-53(Al)/cellulose acetate (CA) mixed matrix membranes. *Sep. Purif. Technol.* **2018**, *199*, 140–151. [[CrossRef](#)]
27. Lai, C.L.; Chen, J.T.; Fu, Y.J.; Liu, W.R.; Zhong, Y.R.; Huang, S.H.; Hung, W.S.; Lue, S.J.; Hu, C.C.; Lee, K.R. Bio-inspired cross-linking with borate for enhancing gas-barrier properties of poly(vinyl alcohol)/graphene oxide composite films. *Carbon* **2015**, *82*, 513–522. [[CrossRef](#)]
28. Alshahrani, A.A.; AlQahtani, M.; Almushaikeh, A.M.; Hassan, H.M.A.; Alzaid, M.; Alrashidi, A.N.; Alsohaimi, I.H. Synthesis, characterization, and heavy-ion rejection rate efficiency of PVA/MWCNTs and Triton X-100/MWCNTs Buckypaper membranes. *J. Mater. Res. Technol.* **2022**, *18*, 2310–2319. [[CrossRef](#)]

29. Deng, L.; Hägg, M.B. Fabrication and evaluation of a blend facilitated transport membrane for CO₂/CH₄ separation. *Ind. Eng. Chem. Res.* **2015**, *54*, 11139–11150. [[CrossRef](#)]
30. Deng, L.; Hägg, M.B. Carbon nanotube reinforced PVAm/PVA blend FSC nanocomposite membrane for CO₂/CH₄ separation. *Int. J. Greenh. Gas Control* **2014**, *26*, 127–134. [[CrossRef](#)]
31. Jahan, Z.; Niazi, M.B.K.; Hägg, M.B.; Gregersen, Ø.W. Cellulose nanocrystal/PVA nanocomposite membranes for CO₂/CH₄ separation at high pressure. *J. Membr. Sci.* **2018**, *554*, 275–281. [[CrossRef](#)]
32. Molki, B.; Aframehr, W.M.; Bagheri, R.; Salimi, J. Mixed matrix membranes of polyurethane with nickel oxide nanoparticles for CO₂ gas separation. *J. Membr. Sci.* **2018**, *549*, 588–601. [[CrossRef](#)]
33. Ghadimi, A.; Gharibi, R.; Yeganeh, H.; Sadatnia, B. Ionic liquid tethered PEG-based polyurethane-siloxane membranes for efficient CO₂/CH₄ separation. *Mater. Sci. Eng. C* **2019**, *102*, 524–535. [[CrossRef](#)] [[PubMed](#)]
34. Deng, J.; Bai, L.; Zeng, S.; Zhang, X.; Nie, Y.; Deng, L.; Zhang, S. Ether-functionalized ionic liquid based composite membranes for carbon dioxide separation. *RSC Adv.* **2016**, *6*, 45184–45192. [[CrossRef](#)]
35. Sodeifian, G.; Raji, M.; Asghari, M.; Rezakazemi, M.; Dashti, A. Polyurethane-SAPO-34 mixed matrix membrane for CO₂/CH₄ and CO₂/N₂ separation. *Chin. J. Chem. Eng.* **2019**, *27*, 322–334. [[CrossRef](#)]
36. Casado-Coterillo, C.; Garea, A.; Irabien, Á. Effect of water and organic pollutant in CO₂/CH₄ separation using hydrophilic and hydrophobic composite membranes. *Membranes* **2020**, *10*, 405. [[CrossRef](#)]
37. Prasad, B.; Mandal, B. Moisture responsive and CO₂ selective biopolymer membrane containing silk fibroin as a green carrier for facilitated transport of CO₂. *J. Membr. Sci.* **2018**, *550*, 416–426. [[CrossRef](#)]
38. Saedi, S.; Madaeni, S.S.; Hassanzadeh, K.; Shamsabadi, A.A.; Laki, S. The effect of polyurethane on the structure and performance of PES membrane for separation of carbon dioxide from methane. *J. Ind. Eng. Chem.* **2014**, *20*, 1916–1929. [[CrossRef](#)]
39. Iovane, P.; Nanna, F.; Ding, Y.; Bikson, B.; Molino, A. Experimental test with polymeric membrane for the biogas purification from CO₂ and H₂S. *Fuel* **2014**, *135*, 352–358. [[CrossRef](#)]
40. Jomekian, A.; Bazooyar, B.; Esmailzadeh, J.; Behbahani, R.M. Highly CO₂ selective chitosan/g-C₃N₄/ZIF-8 membrane on polyethersulfone microporous substrate. *Sep. Purif. Technol.* **2020**, *236*, 116307. [[CrossRef](#)]
41. Santos, E.; Rodríguez-Fernández, E.; Casado-Coterillo, C.; Irabien, Á. Hybrid ionic liquid-chitosan membranes for CO₂ separation: Mechanical and thermal behavior. *Int. J. Chem. React. Eng.* **2016**, *14*, 713–718. [[CrossRef](#)]
42. Galizia, M.; Chi, W.S.; Smith, Z.P.; Merkel, T.C.; Baker, R.W.; Freeman, B.D. 50th anniversary perspective: Polymers and mixed matrix membranes for gas and vapor separation: A review and prospective opportunities. *Macromolecules* **2017**, *50*, 7809–7843. [[CrossRef](#)]
43. Casado-Coterillo, C.; Del Mar López-Guerrero, M.; Irabien, Á. Synthesis and characterisation of ETS-10/acetate-based ionic liquid/chitosan mixed matrix membranes for CO₂/N₂ permeation. *Membranes* **2014**, *4*, 287–301. [[CrossRef](#)] [[PubMed](#)]
44. Casado-Coterillo, C.; Fernández-Barquín, A.; Zornoza, B.; Téllez, C.; Coronas, J.; Irabien, Á. Synthesis and characterisation of MOF/ionic liquid/chitosan mixed matrix membranes for CO₂/N₂ separation. *RSC Adv.* **2015**, *5*, 102350–102361. [[CrossRef](#)]
45. Bernardo, P.; Drioli, E.; Golemme, G. Membrane gas separation: A review/state of the art. *Ind. Eng. Chem. Res.* **2009**, *48*, 4638–4663. [[CrossRef](#)]
46. Fernández-Barquín, A.; Casado-Coterillo, C.; Etxeberria-Benavides, M.; Zuñiga, J.; Irabien, A. Comparison of Flat and Hollow-Fiber Mixed-Matrix Composite Membranes for CO₂ Separation with Temperature. *Chem. Eng. Technol.* **2017**, *40*, 997–1007. [[CrossRef](#)]
47. Casado-Coterillo, C.; Fernández-Barquín, A.; Irabien, A. Effect of humidity on CO₂/N₂ and CO₂/CH₄ separation using novel robust mixed matrix composite hollow fiber membranes: Experimental and model evaluation. *Membranes* **2020**, *10*, 6. [[CrossRef](#)]
48. Ahmadi, M.; Janakiram, S.; Dai, Z.; Ansaloni, L.; Deng, L. Performance of mixed matrix membranes containing porous two-dimensional (2D) and three-dimensional (3D) fillers for CO₂ separation: A review. *Membranes* **2018**, *8*, 50. [[CrossRef](#)]
49. Marcos-Madrazo, A.; Casado-Coterillo, C.; García-Cruz, L.; Iniesta, J.; Simonelli, L.; Sebastián, V.; Encabo-Berzosa, M.D.M.; Arruebo, M.; Irabien, Á. Preparation and identification of optimal synthesis conditions for a novel alkaline anion-exchange membrane. *Polymers* **2018**, *10*, 913. [[CrossRef](#)]
50. Casado, C.; Ambroj, D.; Mayoral, Á.; Vispe, E.; Téllez, C.; Coronas, J. Synthesis, swelling, and exfoliation of microporous lamellar titanosilicate AM-4. *Eur. J. Inorg. Chem.* **2011**, *4*, 2247–2253. [[CrossRef](#)]
51. Rubio, C.; Murillo, B.; Casado-Coterillo, C.; Mayoral, A.; Téllez, C.; Coronas, J.; Berenguer-Murcia, A.; Cazorla-Amoros, D. Development of exfoliated layered stannosilicate for hydrogen adsorption. *Int. J. Hydrog. Energy* **2014**, *39*, 13180–13188. [[CrossRef](#)]
52. Tao, J.; Wang, J.; Zhu, L.; Chen, X. Integrated design of multi-stage membrane separation for landfill gas with uncertain feed. *J. Membr. Sci.* **2019**, *590*, 117260. [[CrossRef](#)]
53. Hussain, A.; Nasir, H.; Ahsan, M. Process design analyses of CO₂ capture from natural gas by polymer membrane. *J. Chem. Soc. Pak.* **2014**, *36*, 411–421.
54. Wijmans, J.G.; Baker, R.W. The solution-diffusion model: A review. *J. Membr. Sci.* **1995**, *107*, 1–21. [[CrossRef](#)]
55. Rezakazemi, M.; Heydari, I.; Zhang, Z. Hybrid systems: Combining membrane and absorption technologies leads to more efficient acid gases (CO₂ and H₂S) removal from natural gas. *J. CO₂ Util.* **2017**, *18*, 362–369. [[CrossRef](#)]
56. Abejon, R.; Casado-Coterillo, C.; Garea, A. Multiobjective Optimization Based on “Distance-to-Target” Approach of Membrane Units for Separation of CO₂/CH₄. *Processes* **2021**, *9*, 1871. [[CrossRef](#)]
57. Robeson, L.M. The upper bound revisited. *J. Membr. Sci.* **2008**, *320*, 390–400. [[CrossRef](#)]

58. Lin, H.; Yavari, M. Upper bound of polymeric membranes for mixed-gas CO₂/CH₄ separations. *J. Membr. Sci.* **2015**, *475*, 101–109. [[CrossRef](#)]
59. Comesaña-Gándara, B.; Chen, J.; Bezzu, C.G.; Carta, M.; Rose, I.; Ferrari, M.C.; Esposito, E.; Fuoco, A.; Jansen, J.C.; McKeown, N.B. Redefining the Robeson upper bounds for CO₂/CH₄ and CO₂/N₂ separations using a series of ultrapermeable benzotriptycene-based polymers of intrinsic microporosity. *Energy Environ. Sci.* **2019**, *12*, 2733–2740. [[CrossRef](#)]
60. Fernández-Barquín, A.; Rea, R.; Venturi, D.; Giacinti-Baschetti, M.; de Angelis, M.G.; Casado-Coterillo, C.; Irabien, Á. Effect of relative humidity on the gas transport properties of zeolite A/PTMSP mixed matrix membranes. *RSC Adv.* **2018**, *8*, 3536–3546. [[CrossRef](#)]
61. Reijerkerk, S.R.; Jordana, R.; Nijmeijer, K.; Wessling, M. Highly hydrophilic, rubbery membranes for CO₂ capture and dehydration of flue gas. *Int. J. Greenh. Gas Control* **2011**, *5*, 26–36. [[CrossRef](#)]
62. Dai, Z.; Deng, J.; Yu, Q.; Helberg, R.M.L.; Janakiram, S.; Ansaloni, L.; Deng, L. Fabrication and evaluation of bio-based nanocomposite TFC hollow fiber membranes for enhanced CO₂ capture. *ACS Appl. Mater. Interfaces* **2019**, *11*, 10874–10882. [[CrossRef](#)] [[PubMed](#)]
63. López Guerrero, M.D.M.; Casado-Coterillo, C.; Irabien, A. Synergistic Effect of Combining Titanosilicate and 1-Ethyl-3-Methylimidazolium Acetate in Mixed Matrix Membranes for Efficient CO₂ Separation. *Eur. J. Sustain. Dev.* **2015**, *4*, 103–112. [[CrossRef](#)]
64. Nguyen, L.N.; Kumar, J.; Vu, M.T.; Mohammed, J.A.H.; Pathak, N.; Commault, A.S.; Sutherland, D.; Zdarta, J.; Tyagi, V.K.; Nghiem, L.D. Biomethane production from anaerobic co-digestion at wastewater treatment plants: A critical review on development and innovations in biogas upgrading techniques. *Sci. Total Environ.* **2021**, *765*, 142753. [[CrossRef](#)]
65. Washim Uddin, M.; Hägg, M.B. Effect of monoethylene glycol and triethylene glycol contamination on CO₂/CH₄ separation of a facilitated transport membrane for natural gas sweetening. *J. Membr. Sci.* **2012**, *423–424*, 150–158. [[CrossRef](#)]
66. Mubashir, M.; Yeong, Y.F.; Lau, K.K.; Chew, T.L. Effect of spinning conditions on the fabrication of cellulose acetate hollow fiber membrane for CO₂ separation from N₂ and CH₄. *Polym. Test.* **2019**, *73*, 1–11. [[CrossRef](#)]
67. Moghadassi, A.R.; Rajabi, Z.; Hosseini, S.M.; Mohammadi, M. Preparation and characterization of polycarbonate-blend-raw/functionalized multi-walled Carbon nano Tubes mixed matrix membrane for CO₂ separation. *Sep. Sci. Technol.* **2013**, *48*, 1261–1271. [[CrossRef](#)]
68. Mubashir, M.; Yeong, Y.F.; Chew, T.L.; Lau, K.K. Optimization of spinning parameters on the fabrication of NH₂-MIL-53(Al)/cellulose acetate (CA) hollow fiber mixed matrix membrane for CO₂ separation. *Sep. Purif. Technol.* **2019**, *215*, 32–43. [[CrossRef](#)]